Multiprobe electron waveguides: Filtering and bend resistances

Harold U. Baranger*
AT&T Bell Laboratories (4G-314), Crawfords Corner Road, Holmdel, New Jersey 07733-1988
(Received 19 June 1990)

Recent work in high-mobility quantum wires suggests that electron waveguide behavior is relevant for transport at low temperature. We therefore study transport in ideal electron waveguides paying particular attention to their multimode properties. In order to address four-probe measurements, junctions between waveguides must be included and we consider systems with both one and two junctions. We find, first, that the junctions strongly filter the electrons, changing the distribution of the electrons among the modes of the waveguide. Second, the junctions give rise to both substantial longitudinal resistance and bend resistances which can be either local or nonlocal. The latter effect is a direct result of the filtering properties and decays on the length scale of a mean free path in a system with disorder. In a system where the disorder is smooth, the decay of the nonlocal bend resistance occurs over a distance much smaller than the transport mean free path but close to the total mean free path. Third, interference in scattering from two junctions leads to an oscillatory dependence of the transmission on the length between the junctions. The period of this oscillation is surprisingly low, being determined by mixing of the various modes in the waveguide, and shows up strongly in the nonlocal resistance. Finally, throughout this work we compare the quantum results to classical calculations in order to separate classical size effects from effects which require coherence. The classical transmission coefficient approach is derived from the Boltzmann equation with suitable boundary conditions. The basic trends are present in the classical calculations; however, there are large quantum deviations in certain cases as well as some phenomena which are strictly quantum mechanical, especially in the few-mode regime.

I. INTRODUCTION

The vast majority of work on electron transport in solids has been concerned with transport through imperfect medium involving scattering, either in a classical context as in the Boltzmann equation or more recently to address quantum fluctuations. However, in recent years advances in materials growth and microfabrication have allowed one to approach a regime of transport in which the effects of imperfections in the solid are small and the main influence comes from geometrical features.[1] The material of choice in this regard is the two-dimensional electron gas which is created at the $GaAs/Al_xGa_{1-x}As$ interface in modulation-doped heterostructures in which, in addition, extremely narrow wires can be made. Studies of transport in these "quasi-one-dimensional ballistic microstructures" have revealed many novel features.[1]

Low-temperature transport in these small structures can be characterized by comparing the size of the structures to several length scales. First, the mean free path is largely determined by elastic scattering; in $GaAs/Al_xGa_{1-x}As$ structures this comes from both remote ionized impurities and residual impurities in the channel. The phase coherence length is the length over which the electrons retain phase information and thus the length over which quantum interference occurs. The phase breaking is caused by either interactions among the electrons or interactions with other degrees of freedom in the problem such as phonons. Transport occurs at the Fermi surface in degenerate systems, thus the third length scale is the Fermi wavelength. In $GaAs/Al_xGa_{1-x}As$ heterostructures, the elastic mean free path can be greater than 1 μm, the phase-breaking length can be greater than 10 μm, and the Fermi wavelength is of the order of tens of nanometers.[2,3]

In order to make contact with these experiments, the regime to consider, then, is when the size of the system is less than either the mean free path or the phase-breaking length and is comparable to the Fermi wavelength. As a first approximation in this regime, it seems reasonable to neglect all scattering. In this limit the wires act as electron waveguides[2] and in this paper we address the properties of ideal electron waveguides—perfectly ordered wires whose constant width is on the order of the Fermi wavelength. Recent work suggests that the corrections to this ideal behavior are important for many of the current experimental structures.[4,5] However, we present the results of our study of the ideal case in this paper both in order to suggest what features of the observed phenomena are related to the ideal waveguide behavior and in anticipation that these phenomena will play an even more important role in structures made of future higher-quality materials.

Most transport experiments are done in a four-probe geometry; in the quantum-ballistic regime, then, it is important to consider a network of electron waveguides. In such a network, it is clearly the junctions between the wires that will dominate the transport properties. Thus we are led to study the scattering properties of such junctions in which the crucial quantities are the transmission

and reflection coefficients among the different modes of the waveguide. We first consider a single junction, building on the previous work done in this case,[6–17] and then consider two junctions, a case which has received some attention recently.[18] After discussing the scattering properties of junctions, we turn to the resistance that results from this scattering, which can be calculated using Büttiker's multiprobe Landauer formula.[19]

The main conclusions of this study are, first, that the junctions strongly filter the electrons, changing the distribution of the electrons among the modes of the waveguide. This filtering has a strong dependence on geometry. Second, the junctions give rise to both substantial longitudinal resistance and bend resistances which can be either local or nonlocal. The latter effect is a direct result of the filtering properties and decays on the length scale of a mean free path in a system with disorder. Third, interference between the two junctions leads to an oscillatory dependence of the transmission on the length between the junctions. The period of this oscillation is surprisingly large, being determined by a mixing of the various modes in the waveguide, and shows up strongly in the nonlocal resistance. Finally, throughout this work we carefully compare the quantum results to classical calculations in order to separate classical size effects from effects which require coherence. The basic trends are present in the classical calculations; however, there are large quantitative deviations from the quantum-mechanical results in certain cases as well as some phenomena which are strictly quantum mechanical (especially in the few-mode regime).

After a brief section on calculational methods (Sec. II), the paper discusses the filtering properties of a single junction (Sec. III) and then turns to the local bend resistance (Sec. IV). The properties of double junctions forms the bulk of the paper, starting with filtering and interference in transmission (Sec. V) and then turning to the influence of these effects on the nonlocal and longitudinal resistances (Sec. VI). The Appendixes discuss the derivation of the classical transmission coefficient approach from the Boltzmann equation, the nature of the threshold singularities, and the definition of mean free paths in waveguides. Preliminary results on some of these topics have been discussed previously.[7,20]

II. CALCULATIONAL METHODS

There are three essential ingredients to our quantum-mechanical calculation: the relation between resistance and transmission coefficients,[19,21] the relation of transmission coefficients to the Green function,[22–24] and the recursive calculation of the Green function for the discretized problem.[25]

The resistance of phase-coherent multiprobe structures was addressed by Büttiker,[19] who viewed the problem as a quantum scattering problem between ideal reservoirs in the tradition of Landauer.[21] He related the currents in the leads I_m to the voltages V_n using the transmitted intensities between the reservoirs (T_{mn} for transmission from lead n to m),

$$I_m = \frac{e^2}{h} \sum_n T_{mn}(V_n - V_m) . \quad (1)$$

Here the current in lead m is very naturally the sum of the pairwise currents between leads m and n where the pairwise current is the transmission coefficient (at the Fermi energy) times the difference in voltage or chemical potential of the reservoirs. Note that the dependence on the Fermi velocity and density of states has canceled, as is usual for Landauer-type arguments. Equation (1) was subsequently derived[23,24] from the more traditional Kubo-Greenwood linear-response approach, a derivation which shows that Eq. (1) is valid for arbitrary magnetic field and which gives useful Green-function expressions for the conductance coefficients. Once the transmission intensities are available, one applies the appropriate constraints on the currents in the leads and solves Eq. (1) for the voltages and hence the resistances.[23]

The second ingredient is to relate the transmission coefficients in Eq. (1) to the Green function for the quantum-mechanical scattering problem. Scattering theory shows that the transmission amplitude is related to the Green function simply by projection onto the transverse wave functions in the asymptotic part of the lead $\chi_\nu(y)$,[22,23]

$$|t_{mn}(\mu,\nu)| = \hbar\sqrt{v_\mu v_\nu} \int dy_m \int dy_n' \, \chi_\mu(y_m)\chi_\nu(y_n')G(y_m,y_n') , \quad (2)$$

where the transmission is from mode ν in lead n to mode μ in lead m, and v_ν is the longitudinal velocity of mode ν (at the Fermi energy). In fact, this projection can be done at any point in the lead outside the scattering region since the population of the various transverse states will not change in the ideal lead.

Finally, in order to calculate the Green function numerically, one needs to discretize the continuum problem. The lowest-order finite difference approximation to the derivatives in the Schrödinger equation produces the standard nearest-neighbor tight-binding Hamiltonian on a square lattice[25] for which the Green function must be evaluated. Dyson's equation relates the Green function G of a system in the presence of a perturbation U to the Green function G_0 in the absence of U: $G = G_0 + G_0 U G$. By judiciously choosing the unperturbed system and the perturbation, one can derive recursive relations for the Green functions which correspond to building up the system slice by slice from left to right.[25] For the multilead systems which are of interest here, somewhat more complicated recursive relations must be developed using the same basic idea.[26] In hard-wall square-corner waveguides, wave-function-matching techniques[8,10] are simpler than the recursive Green-function method used here; however, the advantage of the recursive method is the trivial generalization to disordered problems[20] (see Sec. VI) or arbitrary potentials.[27]

The classical calculations also use Eq. (1) to relate resistance to transmission coefficients, but the transmission coefficients are evaluated for classical ballistic particles, as introduced by Beenakker and van Houten.[28]

Tracing the ballistic trajectories between the leads allows one to evaluate the probability of transmission from one lead to another, a quantity exactly comparable to the quantum result. This result can be derived from a Boltzmann-equation approach (Appendix A) in which Fermi-Dirac statistics is assumed but the particles are otherwise treated classically. The distribution function (in the Boltzmann-equation sense) of particles going into the junction region is continuous in **k** space and uniform in angle,[29] which corresponds to the current being equally distributed among the modes in Landauer-type arguments for the quantum case.

We consider also a discrete-classical approach in which only discrete injection wave vectors are included in a classical-trajectory approach as above. The wave vectors included are those whose transverse component corresponds to the allowed modes in the quantum case. In addition to being intuitively appealing, this discrete approach can be derived from a WKB approximation for the Green function used in evaluating the transmission amplitude [Eq. (2)].[30] Thus this discrete-classical approach includes some aspects of the modal properties of the waveguide without including any coherent scattering in the junction region. A more detailed description and justification of our classical and discrete-classical approaches, as well as analytic results for the single-junction cases, are presented in Appendix A.

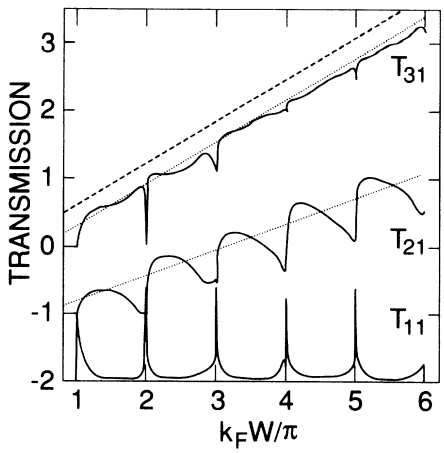

FIG. 1. Total transmission as a function of wave vector for the hard-wall T structure shown in Fig. 2(a) ($W_1 = W_2$). While the average quantum transmission is suppressed from the classical value (dashed line), there is good agreement with a classical calculation in which the total flux is reduced by $\frac{1}{2}$ (dotted line). Deviations from the classical value are particularly strong near the threshold for the transverse subbands ($k_F W = n\pi$). The curves for T_{21} and T_{11} are offset by -1 and -2, respectively.

III. SINGLE JUNCTION: TRANSMISSION PROPERTIES

We start by characterizing the scattering properties of a single junction. Since as discussed above a transport measurement can be regarded as a scattering problem where one injects electrons from reservoirs, it is natural to ask first where does an injected electron go. Previous work has emphasized transmission coefficients between individual low-lying modes;[8,11,12] here we discuss the multimode filtering aspects.

Figure 1 shows the total transmission coefficients, summed over the modes, between the three leads of a T structure shown in Fig. 2(a) (with $W_1 = W_2$). The strength of the scattering at the junction is evident in the deviation of this curve from the step structure expected for ideal quantum point contacts,[31–33] though a weak residual of the first step is present. In fact, the transmission straight through T_{31} and around the bend T_{21} increases linearly with the injected flux while the reflection coefficient T_{11} remains small, as expected classically. The result of the classical calculation (dashed line) always lies above the quantum result. This comes about simply because the quantum zero-point motion in the transverse direction suppresses the amount of injected flux (integer part of $k_F W/\pi$) compared to the classical case ($k_F W/\pi$) for a given Fermi energy. Decreasing the total injected flux in the classical case by $\frac{1}{2}$ brings the two results into agreement. In all future comparisons between the quantum and classical results, we modify the total classical flux in this way.

In order to investigate in more detail where the electrons go, we plot in Fig. 2 the transmission coefficient analyzed by mode $\sum_\mu T(\mu,\nu)$ for both the quantum and discrete-classical (dotted lines) cases. We see that low-lying modes tend to go straight through while the high-lying modes tend to turn the corner in both the classical and quantum-mechanical models. A natural explanation of this general trend is simply that a low-lying mode corresponds to an electron with a forward-directed wave vector which therefore will not see the opening into the side probe, while a high-lying mode corresponds to a transverse-directed wave vector which will see the opening. The quantum results deviate from the discrete-classical ones particularly near the threshold for the modes where more scattering occurs quantum mechanically, leading to both a suppression of the probability to turn the corner and forward transmission in a region where the discrete-classical transmission is zero.

Individual injection modes are not directly accessible in a transport experiment, so rather than asking where an electron injected into a certain mode goes, it makes more sense to study the distribution of electrons among the outgoing modes given that electrons were injected uniformly into all modes. This then characterizes a junction as a filter of electrons. For three transmission coefficients, Figs. 2(d)–2(f) show the quantity $\sum_\nu T(\mu,\nu)/T$, which is essentially the distribution of current among the modes. After going straight through [Fig. 2(e)] the electrons preferentially populate the low-lying modes while after injection down the side arm [Fig. 2(d)] the electrons tend to be in the high-lying modes. In the third case of turning the corner into the side probe, the population of the lowest mode is suppressed. The results of the discrete-classical model yield these same trends, though as above there are deviations connected

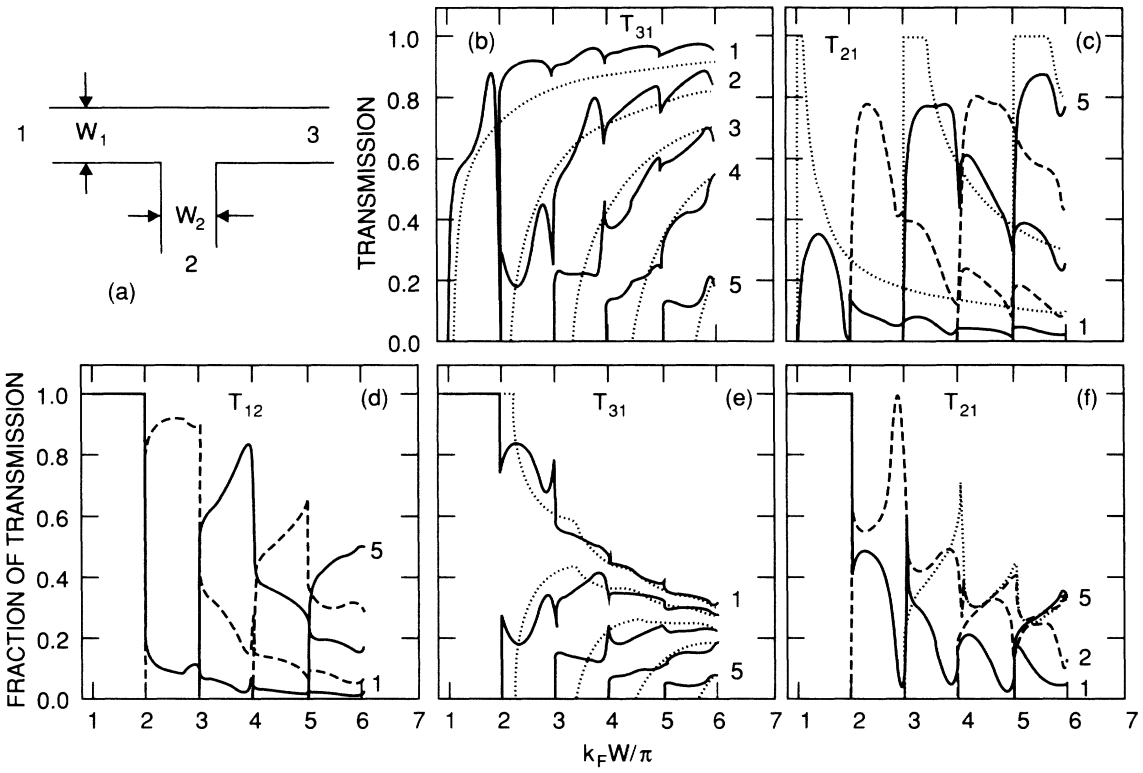

FIG. 2. Transmission coefficients by mode as a function of wave vector for the hard-wall T structure. Quantum results are shown as solid and dashed lines, discrete-classical results as dotted lines. (a) Schematic of the T structure; here $W_1 = W_2$. Panels (b) and (c) show transmission from mode ν (indicated on the right, 1–5) into all modes. (b) Straight through $\sum_\mu T_{31}(\mu,\nu)$. The quantum-mechanical results follow the discrete-classical trend—low-lying modes tend to go straight through more readily than high-lying modes—but show more transmission just above threshold where the discrete-classical model yields zero transmission. (c) Around the bend, $\sum_\mu T_{21}(\mu,\nu)$. The highest-lying mode turns the corner with a high probability, but is less likely to do so than in the discrete-classical model. Panels (d)–(f) show the distribution among the outgoing modes μ (indicated on the right, 1–5). (d) After injection into the side arm, $\sum_\nu T_{12}(\mu,\nu)/T_{12}$. The highest modes are preferentially populated. (e) After going straight through, $\sum_\nu T_{31}(\mu,\nu)/T_{31}$. The junction has filtered the incoming distribution so that low-lying modes are preferentially populated. (f) After going around the bend, $\sum_\nu T_{21}(\mu,\nu)/T_{21}$. The low-lying modes are suppressed.

with the onset of quantum scattering and the threshold singularities. We see then that simply because of geometrical effects, junctions are effective filters of both classical and quantum-mechanical particles.

The filtering properties of a single junction can be improved by altering the junction geometry. Figure 3(a) shows the filtering properties of a cross while Figs. 3(b) and 3(c) show those for a T structure with a wider side probe ($W_2 = 2W_1$). The distribution of outgoing electrons is somewhat sharpened in the case of forward transmission, but the filtering after injection into the side probe deteriorates. Note the large increase in the region of quantum forward transmission for which the discrete-classical result is zero.

The transmission coefficients have sharp structure at the thresholds for the modes of the waveguides[8] (see Fig. 1). These threshold singularities are a general wave phenomena in scattering problems, occurring not only because of the new scattering channel available (into the threshold mode), but also because of the very long trapping times within the scattering region when scattering near threshold.[34,35] The singularities are clearest in the individual transmission coefficients as shown in Figs. 4 and 5. For the case of quantum-mechanical scattering in waveguides, the form of the threshold singularities is derived in Appendix B and we summarize the results here in terms of the longitudinal wave vector q for the relevant mode. There are three distinct cases for the singularities. First, for scattering out of a threshold mode ν in lead n into mode $\mu \leq \nu$ in lead m, $q_\nu \to 0$,

$$|t_{mn}(\mu,\nu)|^2 \sim q_\nu, \quad \mu < \nu \; ; \tag{3a}$$

$$|t_{mn}(\nu,\nu)|^2 \sim q_\nu^2, \quad m \neq n \; ; \tag{3b}$$

$$|t_{nn}(\nu,\nu)|^2 - 1 \sim q_\nu \; . \tag{3c}$$

Second, the behavior for scattering into a threshold mode μ from a lower open mode $\nu < \mu$ is related to that above by symmetry: simply replace q_ν by q_μ in Eq. (3a) as $q_\mu \to 0$. Finally, for scattering between two open modes ν and μ, at the threshold for a third (higher) mode η,

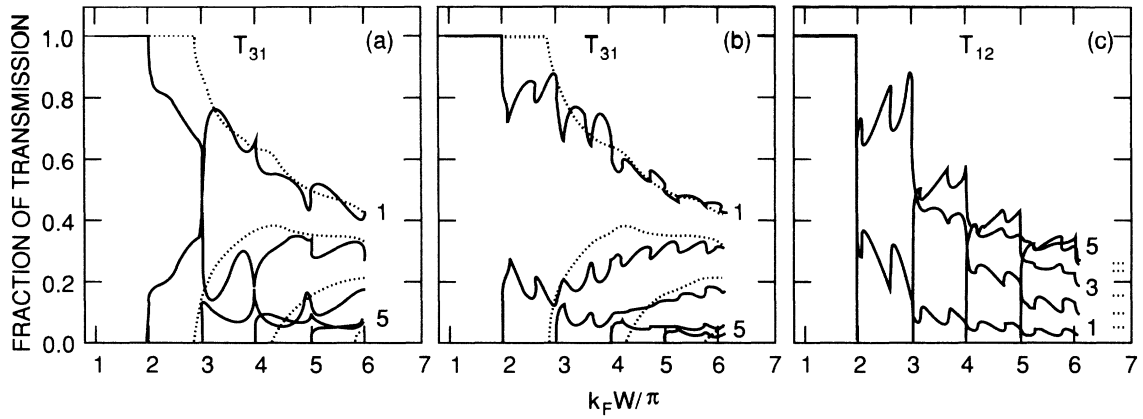

FIG. 3. Distribution among the outgoing modes μ (indicated on the right, 1–5) as a function of wave vector. Quantum results are shown as solid and dashed lines, discrete-classical results as dotted lines (the fifth classical line is zero for the entire range shown). (a) After going straight through a cross section (Fig. 6), $\sum_\nu T_{31}(\mu,\nu)/T_{31}$. Compared to a T structure [Fig. 2(e)], the filtering action is somewhat stronger and the region of quantum transmission in a discrete-classically forbidden region is larger. (b) After going straight through a T structure with $W_2=2W_1$, $\sum_\nu T_{31}(\mu,\nu)/T_{31}$. The filtering action is comparable to that in the cross, but note the larger number of threshold singularities because of the wider side probe. (c) After injection into the side arm of a T structure with $W_2=2W_1$, $\sum_\nu T_{12}(\mu,\nu)/T_{12}$. The enhancement of the high-lying modes is not as great as in the equiwidth T structure [Fig. 2(c)].

$$|t_{mn}(\mu,\nu)|^2 \sim \begin{cases} |t^0_{mn}(\mu,\nu)|^2(1-aq_\eta), & E>E_\eta \quad (4a) \\ |t^0_{mn}(\mu,\nu)|^2(1-b|q_\eta|), & E<E_\eta \quad (4b) \end{cases}$$

as $q_\eta \to 0$. Here E_η is the threshold energy of mode η, a and b are constants that depend on the modes involved, and the superscript 0 on the transmission amplitude denotes its value when $q_\eta=0$. When all the waveguides have the same width asymptotically, Eq. (3c) is modified in the case of the lowest mode: the singularity is order q_1^2 as in the textbook case of reflection from a one-dimensional barrier.

In the case of transmission between two modes at the threshold for a third mode (Fig. 4), the general analysis does not fix the sign of the singularity. There are four possible scenarios depending on the signs of the constants a and b in Eq. (4).[34,35] All four of these situations occur in the transmission coefficients for the T structure (Fig. 4), the nature of the singularity being connected to details of the scattering potential (in our case, the junction). The most naive view of the origin of these singularities suggests the following argument for which type will occur. If the new scattering channel is coupled equally to all the possible outgoing channels, then it will tend to take intensity out of the most likely transmission channel and redistribute it to the less likely ones. The filtering results suggest that the most likely transmission channel is the classical one. Thus one is led to a simple rule of thumb: for a given input mode, the singularity will be a downward cusp on the classically expected transmission channel and an upward cusp on all other channels. We checked this argument on the singularities in the cross, symmetric and asymmetric T structures, and the elbow-bend structure

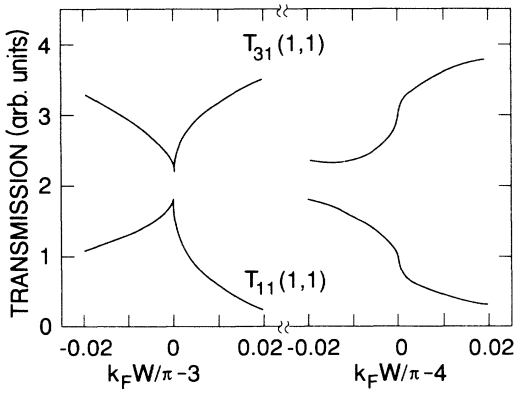

FIG. 4. Examples of the four possible forms of threshold singularities in the case of transmission between two open modes at the threshold for a third mode. The top curves are for transmission straight through a T structure within the lowest mode; the bottom curves are for reflection within the lowest mode (coefficients not normalized).

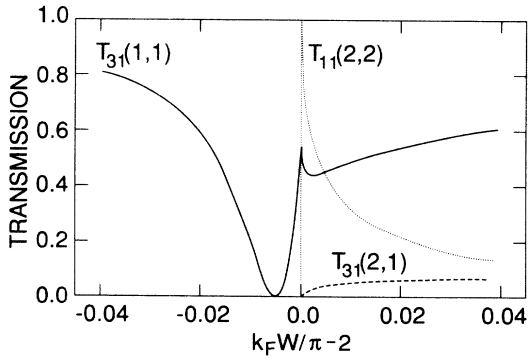

FIG. 5. Transmission coefficients near the threshold for the second mode in a T structure. Note the sharp resonance in the forward transmission within the lowest mode just below threshold and the appropriate singularities in the coefficients involving the second mode.

for all thresholds up to $\eta=8$ for μ and ν up to 7. This rule gave the correct type of singularity about two-thirds of the time. Obviously, this argument is too simple in detail (in particular, singularities of the type shown on the right-hand side of Fig. 4 are predicted never to occur); however, as a rough rule it is surprisingly accurate.

One sharp feature in the transmission coefficients for a T structure is not a threshold singularity since it occurs slightly below the threshold for the second mode [Figs. 1 and 2(b)]. An expanded plot of this feature in Fig. 5 shows that the forward transmission goes essentially to zero for $k_F W/\pi$ just below 2, suggesting that this feature is a resonance. To explain this feature, recall that the cross structure has two bound states in the junction region,[8] one with even symmetry just below the $\nu=1$ continuum and the other one with odd symmetry just below the $\nu=2$ continuum at $k_F W/\pi=1.93$. This second state does not mix with the $\nu=1$ continuum because of symmetry. However, in a T structure the fourfold symmetry is broken and the second state *does* mix with the $\nu=1$ continuum, producing the observed resonance. Because the change from the cross to the T structure is large, a substantial coupling to the former bound state is produced which causes both a large shift in the resonance energy from that for the bound state ($\Delta k \approx 0.065\pi/W$) and a substantial width.

We have discussed the scattering states of a single junction because these are the states relevant for transport. However, true bound states exist in the junction region for these classically unconfined systems: states with energies between the two-dimensional zero of energy and the threshold energy of the first mode will be bound, and for symmetry reasons higher-energy bound states may exist. Such states were studied in a waveguide with a right-angle bend by Lenz *et al.*[6] and more recently in junctions.[8,11,14]

IV. SINGLE JUNCTION: BEND RESISTANCE

The scattering properties discussed in Sec. III cause the junction to have a resistance even in the absence of impurity scattering.[7,9,10,20,36,37] A four-probe measurement that shows this clearly[9,20,36] is indicated schematically in the inset to Fig. 6. Using Eq. (1), the resistance for this situation, which we call the local bend resistance, is

$$R_B = \frac{h}{e^2}\frac{T_{31}-T_{21}}{4T_{21}(T_{31}+T_{21})} . \tag{5}$$

The calculated bend resistance shown in Fig. 6 is particularly large (>10 kΩ) when only one mode is occupied since in this case it is difficult to make the electron wave turn the corner. R_B is still substantial (a few kilo-ohms) in the few-mode number regime, but decays as the number of modes becomes large. The dependence of the bend resistance on k_F within a subband follows directly from the scattering properties above.[9,20] As the energy increases from just above threshold to just below the next threshold, all of the modes become more low lying. Classically, the **k** vector of the electrons becomes more forward directed as the energy increases for fixed mode

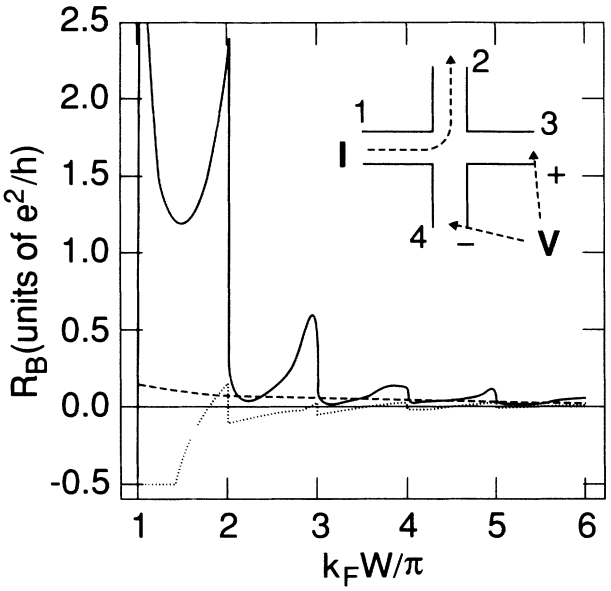

FIG. 6. Bend resistance, defined in the inset, as a function of wave vector in the low mode number regime. The quantum result (solid line) can be much larger than the classical result (dashed line) and decreases sharply at the onset for a mode. A discrete-classical model (dotted line), which includes subband structure but not coherence in the junction region, shows singularities at thresholds but is in poor agreement for the magnitude.

number. Hence T_{31} increases compared to T_{21} and the bend resistance increases. Rapid variation of the bend resistance as the number of modes changes has recently been observed experimentally.[38]

The importance of the quantum-mechanical nature of the scattering is apparent from the differences between the quantum, classical, and discrete-classical calculations in the few-mode regime. While the classical calculation gives roughly the correct magnitude, the quantum results shows structure near the threshold for the modes and has an average value much higher than the classical one in the few-mode regime. The discrete-classical calculation introduces structure at the thresholds for the modes; however, this structure is not of the correct magnitude and leads to the wrong sign for R_B. Thus the structure in the quantum calculation is not simply a result of the modes in the wires but rather depends on coherent scattering in the junction itself. As the number of modes increases, the absolute differences between the three calculations diminish, but the quantum effects still produce a substantial fractional change in R_B compared to the classical value.[9]

V. DOUBLE JUNCTION: TRANSMISSION PROPERTIES

We have seen that a single junction between ballistic wires acts as a filter. In the quantum regime this corresponds to a selective population of the modes of the waveguide; in the classical regime, the angular distribution of transmitted electrons is not isotropic. In the con-

text of multiprobe structures, it is natural to ask how these filtering properties change when two junctions are present in the ballistic region. We will see that additional quantum effects should be present in the coherent case because of the interference between the scattering at the two junctions.

A. Dependence on energy: filtering

It seems intuitively clear that one should be able to improve the selectivity of a junction filter by simply having two junctions, as shown in the inset to Fig. 9. We investigate the filtering properties of such four-probe systems in Fig. 7, first for a fixed separation of the junctions ($L=2W$) and then averaged over a wide range of separations. Comparing this to the single junction case in Fig. 2, we see that only a modest improvement in filtering properties is obtained, no more than was obtained by modifying the single-junction geometry (Fig. 3). While quantum interference effects do show up as small rapid oscillations in the case of fixed L, it seems difficult to take advantage of these interference effects to substantially improve the filtering properties because of their small width in energy. Averaging over many different structures [Figs. 7(b) and 7(c)] smooths these oscillations, but the structure at the mode thresholds coming from the transverse coherence is retained. As in the single-junction case, the overall trends in the filtering behavior are predicted by a classical ballistic model (not shown). The case of transmission between the two side probes (T_{24}) is notable as this is a way to enhance the relative population of the mid-lying modes.

B. Dependence on length: interference

The clearest examples of quantum interference in the scattering from the two junctions comes, not surprisingly, in the single-mode limit. In this regime the double junction is in many ways analogous to the optical Fabry-Pérot cell. One expects oscillations in the transmission properties of the structure as a function of system parameters such as the length between the probes, the magnetic field,[2,39] or the Fermi energy. Because it is the simplest case, we will study the oscillations as a function of length between the probes. However, all of these system parameters affect the transmission by changing the phase relations among the different scattered waves; thus we suggest that the qualitative features discussed will be present when any of the system parameters is varied. Recently, a way of moving a probe along a high-mobility two-dimensional electron gas has been presented.[40,41]

The results in the single-mode regime are shown in Fig. 8 for three different energies: near threshold, for $k_{\parallel}=k_{\perp}$, and just below the second threshold. All three cases show the expected period $P=\lambda_{\parallel}/2=\pi/k_{\parallel}$. The high reflection from a single junction in the two cases near thresholds (a and c, see Fig. 1) produces high average reflection and sharp transmission resonances in the double-junction characteristics.

The unusual phase relations among the different transmission coefficients is of particular interest. In simple one-dimensional Fabry-Pérot or resonant tunneling situations, the transmission through the structure and the reflection are exactly out of phase since their sum is fixed by unitarity. In waveguide structures, however, only the transmission out of all the leads is fixed. The simple situation is realized in Fig. 8(c) (once evanescent wave effects are suppressed). In the case of the lowest energy [Fig. 8(a)], while the transmission straight through and the reflection are roughly out of phase as expected, the transmission around the first bend (T_{41}) has a curious sawtooth behavior. In the symmetric case, $k_{\parallel}=k_{\perp}$ in Fig. 8(b), the transmission straight through and the reflection are actually in phase while both are out of phase with the transmission around the first bend.

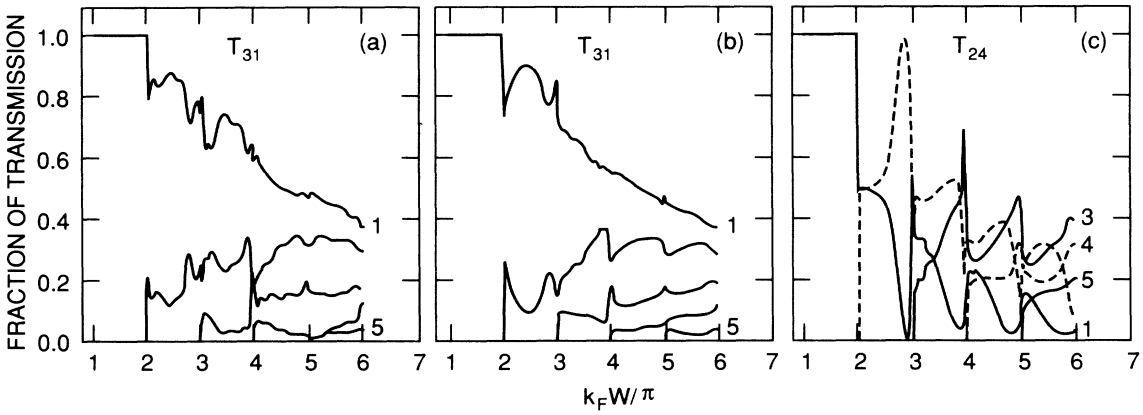

FIG. 7. Distribution among the outgoing modes μ (indicated on the right, 1–5) as a function of wave vector for a double-junction structure. (a) After going straight through for fixed $L=2W$, $\sum_{\nu} T_{31}(\mu,\nu)/T_{31}$. The filtering action is comparable to that in a single-junction cross, but additional oscillations occur because of coherence between the two junctions. (b) After going straight through, averaged over L in the interval $[1.4W,7.4W]$. (c) After turning two corners, averaged over L in the interval $[1.4W,7.4W]$, $\sum_{\nu} T_{24}(\mu,\nu)/T_{24}$. The mid-lying modes are preferentially populated. A solid line is used for modes 1, 3, and 5, a dashed line for modes 2 and 4.

In a multimode situation, the effect of interference on the transmission should be more complicated because the longitudinal wavelengths of the different modes differ. In fact, it has been shown that such multimode interference sharply degrades the performance of quantum stub tuners which must therefore be used in the single-mode regime.[12] In the two mode case shown in Fig. 9, it is somewhat surprising, therefore, that a large periodic modulation is still present. More surprising is the fact that the periodicity with the largest amplitude does not correspond to either of the two $k_{\|}$. It is the small-amplitude high-frequency oscillation in T_{41} and T_{44} that corresponds to $k_{\|}$ for the second mode and an oscillation at $k_{\|}$ for the lowest mode is hardly present at all. The average value of the transmission coefficients is approximately the classical value, which does not vary with length.

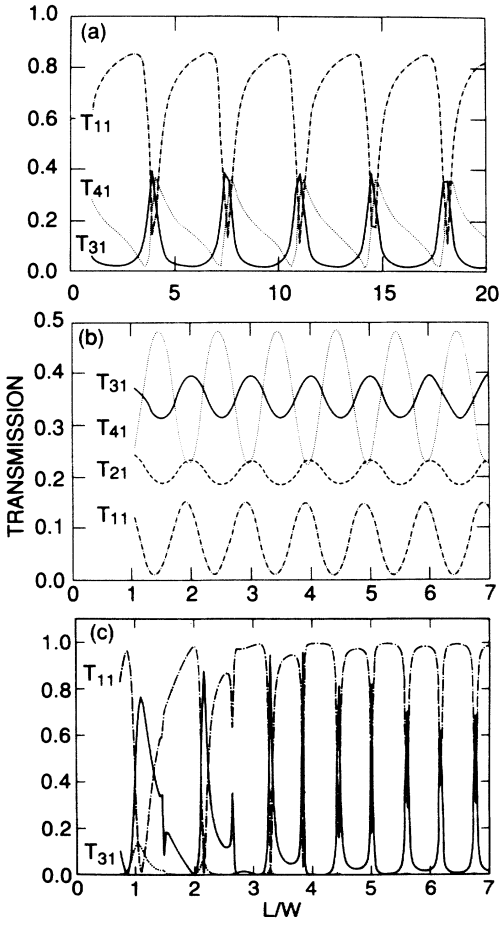

FIG. 8. Transmission coefficients in the lowest subband for a two-junction structure (inset to Fig. 9) as a function of the length between the junctions. Transmission straight through (T_{31}, solid), out the first side probe (T_{41}, dotted), out the second side probe (T_{21}, dashed), and reflected (T_{11}, dash-dotted) are shown. (a) $k_F W/\pi=1.04$. The junctions are highly reflecting and transmit only on resonance; however, the transmission out the first side probe has an unusual sawtooth behavior. (b) $k_F W/\pi=\sqrt{2}$. The reflection and forward transmission are *in phase* while both are out of phase with the transmission out the first side probe. (c) $k_F W/\pi=1.99$. The junctions are again highly reflecting and transmit only on resonance.

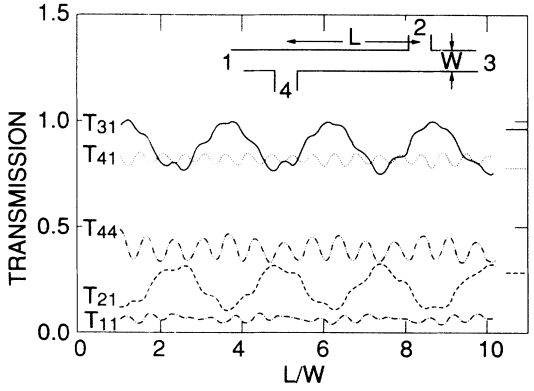

FIG. 9. Transition coefficients at $k_F W/\pi=2.5$ for a two-junction structure (inset) as a function of the length between the junctions. In addition to the coefficients shown in Fig. 8, the reflection after injection into a side probe (T_{44}) is shown as dash-double-dotted. The short period modulation caused by the two longitudinal wave vectors (evident in T_{41} and T_{44}) beat with each other to produce large-amplitude large-period oscillations in the forward transmission. The classical values for the transmission coefficients, which do not depend on L, are shown as tick marks.

The large-amplitude oscillation occurs at the *mixing* frequency between the two modes, corresponding to $k_{\|,1}$-$k_{\|,2}$ and caused by the intermode reflection of the junctions. Because the transmission properties of the junction depend strongly on longitudinal wavelength, the amplitudes of the different periods present will differ. The mixing period has the largest amplitude because the junctions are much less transparent to the mixed wave (longer longitudinal wavelength) then they are to the fundamental $k_{\|}$ causing interference between these mixed waves to build up.

For the cases of three, five, and eight modes, Fig. 10 shows the transmission as a function of junction separation in the insets and the Fourier power spectra[42] of the straight-through transmission in the main part of the figure. First note that as the number of modes increases the amplitude of the oscillations decreases rapidly for T_{11} and T_{41}, while surprisingly the amplitude does not decrease rapidly for T_{31} or T_{21}. As before the average value of the transmission is approximately the classical length-independent value (tick marks). The power spectra show very clear sharp peaks for $M=3$ and 5, which agree very well with the mixing frequencies. The highest amplitude occurs for mixing of midlying modes since low-lying modes do not reflect while high-lying modes have a low transmission through the first junction. In the case of eight modes, the peaks in the power spectra are broader, and though in qualitative agreement with the mixing prediction, it is difficult to separate the influence of the individual mixing frequencies as they are very closely spaced.

While we have been emphasizing a quantum-mechanical explanation for the surprising behavior of the transmission coefficients in the double junction, the per-

sistence of the oscillations to a high mode number suggests that a classical effect may be involved. The classical model discussed above, in which the distribution function for incoming particles is isotropic, does not produce any oscillations in the transmission coefficients. However, the discrete-classical model, in which injected particles are restricted to fixed angles corresponding to the transverse modes, does predict oscillations. The filtering of the first junction sets up a "beam" of particles in the strip between the junctions which then either goes through the second junction or turns the corner depending on L. This mechanism produces a period of $P=2Wk_{\parallel}/k_{\perp}$ for each mode. These periods do not match the calculated periods in the few-mode regime (and do not predict the correct dependence on Fermi energy). Such periods may be contributing to the broad peaks in the eight-mode case; however, the discrete-classical predictions do not agree with the numerical results as well as the quantum predictions even in this case.

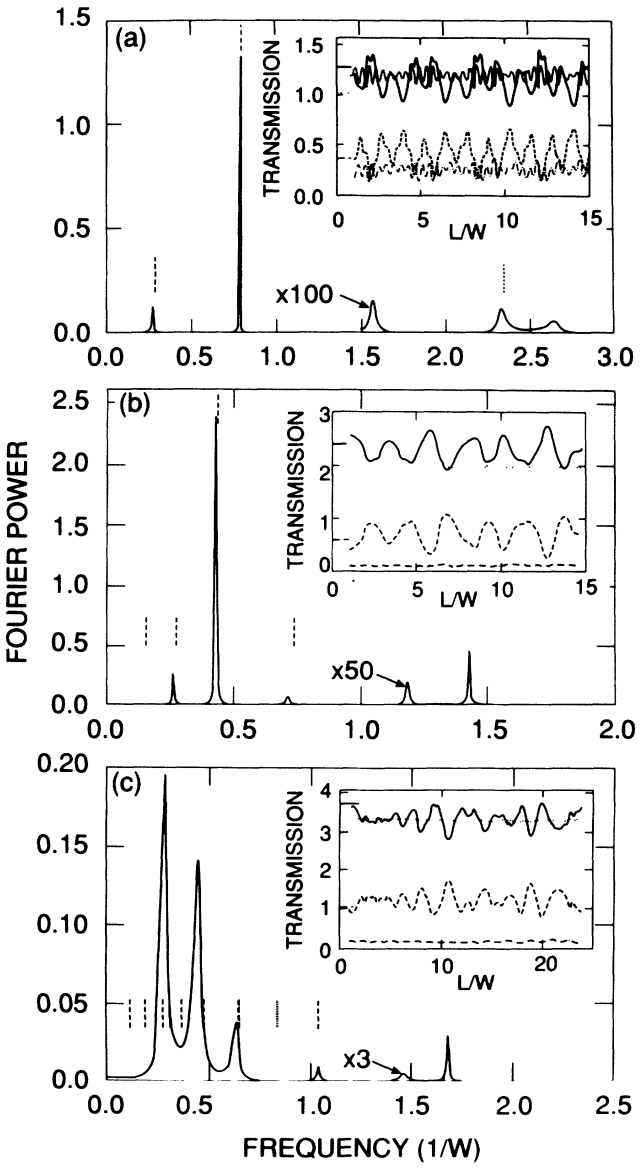

FIG. 10. Fourier power of the forward transmission coefficient in a two-junction structure. Dashed lines mark the difference frequencies of nearest-neighbor subbands; dotted lines those of further separated subbands. The insets show the transmission coefficients as a function of the length between the junctions; transmission straight through (T_{31}, solid), out the first side probe (T_{41}, dotted), out the second side probe (T_{21}, dashed), and reflected (T_{11}, dash-dotted) are shown. (a) $k_F W/\pi=3.5$. Power is peaked at the two nearest-neighbor difference frequencies. There is some power at the difference between the first and third modes (dotted line) and at this frequency mixed with the two nearest-neighbor difference frequencies. (b) $k_F W/\pi=5.5$. Power is peaked at several of the main difference frequencies. (c) $k_F W/\pi=8.5$. Power is peaked in the general vicinity of the difference peaks, but individual peaks cannot be resolved.

VI. DOUBLE JUNCTION: NONLOCAL AND LONGITUDINAL RESISTANCES

In the four-probe double-junction structures that we are considering, two distinct resistances can be defined (in the absence of a magnetic field) as in the insets to Figs. 11 and 12: the familiar longitudinal resistance and the nonlocal bend resistance[7,37] (which has also been called a transfer resistance[28,43]). Applying Büttiker's multiprobe Landauer formula,[19] Eq. (1), we express these resistances in terms of transmission coefficients as

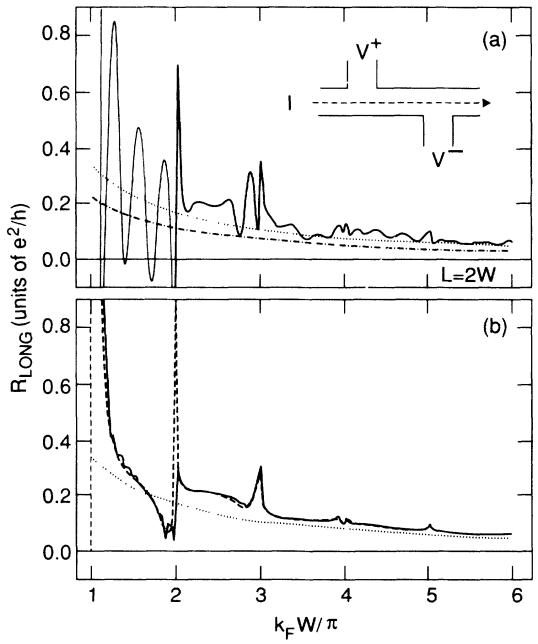

FIG. 11. Longitudinal resistance (defined in inset) as a function of wave vector for a two-junction structure. (a) $L=2W$. (b) Averaged over L in the interval $[1.4W,7.4W]$. The full quantum result (solid) contains large interference effects absent from either the classical result (dotted) or the cascaded-single-junction quantum result (dashed). Equilibration of the electrons between the junctions in the classical model produces a small decrease in magnitude (dash-dotted).

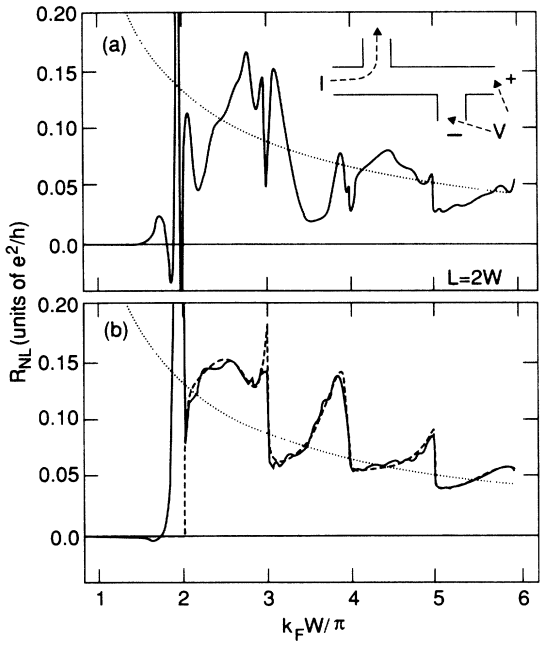

FIG. 12. Nonlocal bend resistance (defined in inset) as a function of wave vector for a two-junction structure. (a) $L=2W$. (b) Averaged over L in the interval $[1.4W, 7.4W]$. The full quantum result (solid) contains large interference effects absent from either the classical result (dotted) or the cascaded–single-junction quantum result (dashed). Equilibration of the electrons between the junctions eliminates the nonlocal bend resistance in both the classical and quantum cases, showing that R_{NL} is a filtering and coherence effect. The nonlocal effect is small in the single-mode quantum case because redistribution of the electrons among the modes is not possible.

$$R_{LONG}=(h/e^2)(T_{21}^2-T_{41}^2)/D\ , \tag{6}$$

$$R_{NL}=(h/e^2)(T_{31}T_{24}-T_{21}^2)/D\ , \tag{7}$$

where

$$D=(T_{41}+T_{21})[2T_{31}T_{24}+(T_{31}+T_{24})(T_{21}+T_{14})+T_{21}^2+T_{41}^2]\ .$$

Because of the dependence of the transmission coefficients on both the energy and the length between the junctions, it is not surprising that these resistances also depend on these parameters.[18] There are several possible sources for energy- and length-dependent resistances: the classical scattering properties of a ballistic junction, classical filtering, waveguide effects either in terms of mode structure or modified single-junction properties, and, finally, coherence between the two junctions. In the following discussion, we will try to separate out these various effects by considering several different classical and quantum calculations.

A. Dependence on energy: filtering

The dependence of R_{LONG} and R_{NL} on the Fermi wave vector is shown in Figs. 11 and 12, respectively. Five different calculations are compared. First, the quantum result at a fixed junction separation and, second, averaged over many junction separations is the solid line in panels (a) and (b), respectively. Third, the classical resistance of the double junction (obtained from an isotropic distribution function at injection) is independent of L and decreases smoothly as $k_F W$ increases (dotted line). The classical transmission coefficients used here are obtained from following many classical trajectories through the double-junction structure,[28] as discussed in connection with Figs. 9 and 10 and in Appendix A.[44] The final two curves result from "cascading" the single-junction results, either classical (dash-dotted) or quantum (dashed). In the classical case, this involves approximating the double-junction transmission properties by a product of the appropriate single-junction transmission coefficients so that all filtering properties of the first junction are discarded (complete equilibration). In the quantum case, a product of single-junction transmission coefficients is also used; however, the mode structure is retained so that filtering is included (no equilibration between the modes). (Reflection from the second junction is assumed to go back through the first junction and out the horizontal lead.) Thus ballistic single-junction effects are given by the classical cascaded–single-junction result, classical filtering effects by the full classical calculation, quantum mode or single-junction effects by the quantum cascaded–single junction result or the double-junction averaged over L, and finally double-junction coherent effects by the full quantum calculation. There are close analogies between the various approaches used here and those used in the resonant tunneling problem; in particular, the cascaded–single-junction results correspond to sequential tunneling either with preservation of the transverse momentum distribution (no equilibration of modes, our quantum cascaded single junction) or with relaxation of the transverse momentum distribution (equilibration of modes, our classical cascaded single junction).[45]

In the case of the longitudinal resistance (Fig. 11), at fixed L one sees the interference between the junctions clearly in the full quantum calculation when one mode is occupied ($k_F W/\pi<2$).[18] The classical cascaded–single-junction result (which includes equilibration) gives the correct order of magnitude for R_{LONG}, showing that this resistance is largely a ballistic single-junction effect. The full classical calculation yields a somewhat larger resistance in better agreement with the quantum result, showing that R_{LONG} is enhanced by filtering. However, the classical calculations do not, of course, reproduce the considerable structure in the quantum result, which in the low-mode number regime can be a 100% effect. Note in particular that $R_{LONG}<0$ for certain parameters when $M=1$. When averaged over many junction separations, the full quantum result agrees with the quantum cascaded–single-junction result (without equilibration) and shows a small average deviation from the classical result as well as structure near the thresholds for the modes. These deviations, then, are the result of coherence within a single junction: mode structure and quantum filtering.

The results for the nonlocal bend resistance (Fig. 12) differ from those for R_{LONG} most obviously in that the

classical cascaded–single-junction result for R_{NL} is identically zero, as can seen from Eq. (7) expressing the double-junction transmission coefficients as products of the single-junction coefficients. Thus the nonlocal bend resistance is entirely a filtering and coherence effect. As we found for R_{LONG}, the full classical result gives approximately the correct magnitude of R_{NL}, but misses a great deal of structure due to coherence either within a single junction or between the two junctions. The structure near the threshold of the modes caused by coherent single-junction scattering [as seen in the quantum cascaded–single-junction result or full quantum result averaged over L of Fig. 12(b)] is larger in the case of R_{NL} than in R_{LONG}. Deviations from the classical result coming from coherence between the two junctions are clear in the full quantum result at fixed $L=2W$ in Fig. 12(a). In the quantum calculations, R_{NL} is small when only one mode is occupied ($k_F W/\pi<2$) since no filtering can take place except through evanescent modes. In fact, in the cascaded–single-junction case where no evanescent effects are included, R_{NL} is exactly zero in the single-mode regime.

The close connection between filtering and the nonlocal bend resistance indicated by the calculations (Fig. 12) is also clear qualitatively. The nonlocal bend resistance measures the difference between the transmission into lead 2 and the transmission into lead 3 after going through the first junction [Eq. (7)]. For injection from lead 1, the first junction preferentially populates the low-lying modes causing preferential transmission into lead 3, $T_{31}>T_{21}$. For injection from lead 4, the first junction preferentially populates the high-lying modes causing preferential transmission around the bend into lead 2, $T_{24}>T_{34}=T_{21}$. Hence, from Eq. (7), R_{NL} is positive. A similar argument shows that filtering should increase the magnitude of R_{LONG}: usually $T_{41}>T_{21}$ with or without equilibration (simply because two junctions are involved in T_{21}, see Figs. 9 and 10) and filtering acts to decrease further T_{21} since the low-lying modes are preferentially populated after the first junction.

B. Dependence on length: interference

The coherent double-junction contribution to these resistances is most easily seen in the dependence on the separation between the junctions shown in Fig. 13. As in the case of the transmission properties, this is the simplest way of changing the phase relations between the scattered waves; other ways of varying these phase relations which are easier to realize experimentally (i.e., a weak magnetic field[2,39]) are expected to give qualitatively similar results. The full classical results do not depend on L and are marked on the resistance axis. They roughly agree with the average of the quantum results except in the single-mode case [Fig. 13(a)] where R_{NL} is zero because no filtering is possible. For the smallest L, the quantum R_{NL} is nonzero because of coupling between the junctions through evanescent modes and is opposite in sign to the classical prediction.

In the multimode case, both resistances show oscillations caused by coherence. The most striking result is the large-amplitude oscillations in R_{NL} (larger than those in R_{LONG}) which occur at the mixing frequencies. Equation (7) shows that R_{NL} is related to those transition coefficients which show the mixing behavior strongest, T_{31} and T_{21} (see Figs. 9 and 10). It is surprising that the oscillations remain large and at low frequencies even in the $M=8$ case. These oscillations at the mixing frequencies in both R_{LONG} and R_{NL} may explain the observation of unexpected periodicities in the magnetoresistance of high-mobility GaAs/Al_xGa_{1-x}As wires which could not be simply related to geometric features.[46]

C. Decay in the presence of disorder

Throughout this paper we have been discussing the properties of ideal electron waveguides; however, scattering processes will be present in real wires, particularly the elastic scattering caused by impurities. One expects elastic scattering to degrade the ballistic effects, and hence R_{NL}, on a length scale of the order of the elastic mean free path.[47] In fact, previous work[20] has shown that for short-range scatters (δ functions that are s-wave scatter-

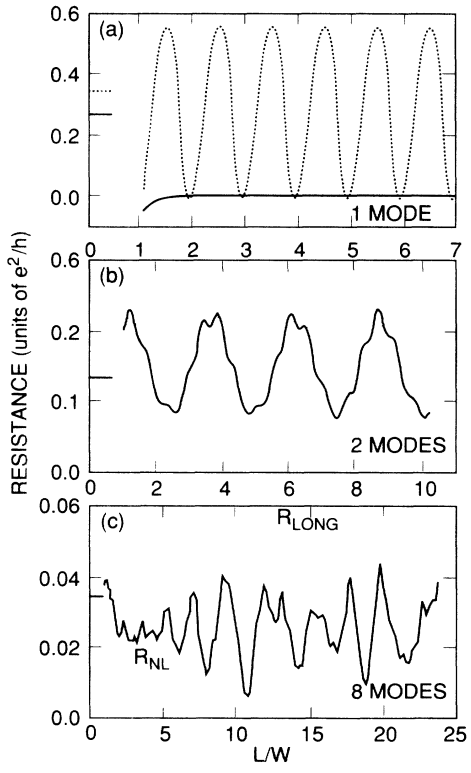

FIG. 13. Longitudinal (dotted) and nonlocal bend (solid) resistances as a function of the separation between the junctions for different energies. Classical values are independent of length and indicated on the left. (a) $k_F W/\pi=\sqrt{2}$. R_{LONG} has large oscillations with a period of the longitudinal wavelength, while R_{NL} is nearly zero because only one mode is occupied. (b) $k_F W/\pi=2.5$ Large-amplitude oscillations of R_{NL} occur at the mixing frequency. (c) $k_F W/\pi=8.5$. The average resistances are close to the classical values, but large deviations remain especially in the nonlocal bend resistance.

ers) R_{NL} decays exponentially on a scale of approximately the mean free path. However, the experimental result in $GaAs/Al_xGa_{1-x}As$ modulation doped structures is that R_{NL} decays much more rapidly than the transport mean free path obtained from the mobility.[7,37,48] It was suggested[7] that this arises from the smooth nature of the scattering potential in this system (most of the impurities are in the modulation doped layer, not the conducting channel), which because of the non-s-wave scattering causes a large difference between the transport mean free path l_{tran} (which contains a $1-\cos\theta$ weighting in bulk), and the total mean free path l_{tot} (which is simply an isotropic average in bulk).[49] Since R_{NL} is sensitive to the filtering properties of the junction, it is degraded by forward scattering which will not degrade the mobility, so that one expects R_{NL} to decay on the scale l_{tot}.

We test this idea by calculating R_{NL} in the presence of a smoother scattering potential than that used in Ref. 20. Recently, attention has been paid to the evaluation of scattering in realistic potentials.[4,5] We do not use a realistic potential but simply generalize the usual Anderson model for disorder: instead of choosing a random potential-energy value on each site we choose a random value on every fifth site and linearly interpolate in between. Appendix C shows that both l_{tot} and an analog of l_{tran}, the backscattering mean free path l_{bs},[5] can be defined in waveguides (within the Born approximation) and can be evaluated by finding the transmission through slices of the waveguide.

Figure 14 shows the decay of R_{NL} as a function of junction separation for a case when $l_{tot}\approx 6.4W$ and $l_{bs}=56W$.[50] The solid line shows R_{NL} averaged over many impurity configurations while the error bars indicate the statistical uncertainty in this mean. Clearly, R_{NL} decays on a length scale of order l_{tot} rather than l_{bs}, confirming the ideas suggested in Ref. 7. Note, however, that the decay is somewhat slower than exactly l_{tot}.[51] The sample-to-sample fluctuations of R_{NL} about the mean shown in Fig. 14 are, of course, nonlocal over the entire phase-coherence length.[47]

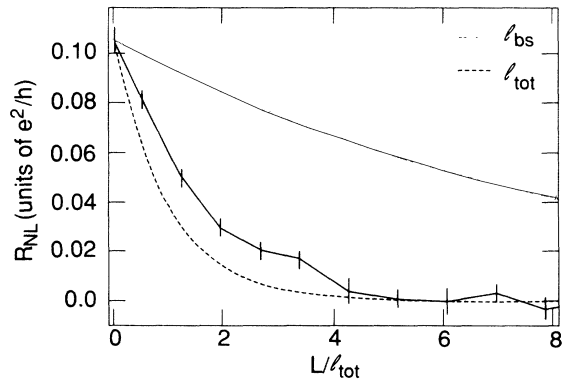

FIG. 14. Decay of the nonlocal bend resistance as a function of junction separation in the presence of disorder (solid) compared to an exponential decay with length scale l_{tot} (dashed) or l_{bs} (dotted). The smooth impurity potential produces a substantial difference between the backscattering and total mean free paths. The length scale for the decay of R_{NL} is of the order of l_{tot} and is certainly much less than l_{bs}.

VII. CONCLUSIONS

In presenting the properties of single and double junctions between ideal electron waveguides, the emphasis in this paper has been on multimode aspects. The first conclusion is that these junctions act as crude filters: while the current injected from the reservoirs in a transport measurement is uniformly distributed among the modes, after a junction the distribution of current is not uniform. In fact, depending on which probes are used, the low-lying modes (forward transmission), high-lying modes (injection down the side arm of a T structure), or mid-lying modes (transmission between the two side arms of the double-junction structure) can be preferentially populated. However, the filtering in these simple structures, while substantial, is not extremely good and it seems that more complicated structures need to be considered if one is to create good electron filters.

The scattering properties of the junctions cause them to have definite resistance. This bend resistance can be either local, as in R_B of a single junction and R_{LONG} of the double junction, or manifestly nonlocal, as in R_{NL}. The nonlocal bend resistance depends crucially on having ballistic electrons and is caused essentially by the filtering properties of the junctions. The extent of the nonlocality in the mean R_{NL} is given by the total mean free path which can be much smaller than the transport mean free path in a smooth scattering potential.

Coherence between the two junctions results in oscillations of the transmission coefficients and the bend resistances as a function of the length between the probes. These oscillations do not occur at the expected values related to the longitudinal wavelengths, but rather at periods corresponding to mixing of the various modes. As the number of modes gets larger, the oscillations at the mixing frequencies are more pronounced in those transmission coefficients which involve both junctions and in the nonlocal bend resistance.

Throughout this work, the full quantum results have been compared to classical calculations. The classical calculations are accurate in predicting the trends in the average quantum behavior. The quantum deviations arise from two sources: first, coherence on the scale of the width of the wires which produces mode structure and coherent single-junction scattering, and second, coherence between the two junctions. The first source causes structure in the transmission coefficients at the mode thresholds, which shows up as sharp structure in the bend resistances. The second source causes oscillations as a function of wavevector or length between the junctions and show up particularly in the nonlocal bend resistance, as noted above. In terms of magnitude, the quantum deviations in these structures are not small: even in the multimode regime, the threshold structure in the bend resistances or the oscillations in the nonlocal bend resistance are of order the average (classical) resistance. In the single-mode regime, of course, quantum effects dominate.

The waveguides used for most of this study are ideal waveguides—the walls are infinite hard walls, the potential inside is constant, and the corners are square. However, experimental quantum wires will, of course, be imperfect in each of these aspects—the walls are soft,[52] the impurities lead to a random potential,[4] and the corners are rounded.[27] The role of these realistic aspects of the potential have been been considered with regard to quantum point contacts,[53] boundary scattering,[54] and the suppression of the low-field Hall resistance.[27,28,43] The qualitative conclusions of the present work should hold for some of these imperfect structures since they seem to be very general: junctions will filter the electrons causing bend resistances as long as the total mean free path is large enough and a substantial fraction of the electrons is not randomly scattered by the junction. Of course, the quantitative conclusions may change quite a bit; one of the more interesting changes recently noted is the existence of increased quantum fluctuations in junctions with rounded corners[30,55] connected to the irregular classical paths in the junction region.[28,30,56]

Finally, the bend resistances, both local and nonlocal, were first studied in more complicated structures in which there were several junctions,[7,37] and we wish to make an explicit connection to these more complicated situations. In the work of Timp *et al.*,[7] the two leads used for measuring voltage were fixed while the path of the current through the structure was changed from being straight through to being bent either at one of the voltage probes or away from them. The reciprocity relations for multiprobe transport[19] show that this measurement is equivalent to keeping the current path fixed through the two original voltage probes while measuring two voltage differences with the original current probes (straight through and bent). Subtracting these two voltages yields the voltage measured with two probes joining at the same junction thus differences in the resistances in Ref. 7 correspond to what we have been called the bend resistances. Of course, the scattering region is more complicated in the structures of Timp *et al.* and Takagaki *et al.* because of the additional junctions; however, the essence of the nonlocal bend resistance remains filtering of ballistic particles.

ACKNOWLEDGMENTS

I thank E. Gerjuoy, F. M. Peeters, A. D. Stone, and G. Timp for many valuable discussions.

APPENDIX A: CLASSICAL TRANSMISSION COEFFICIENTS

In this appendix, we find the resistance of a ballistic junction attached to reservoirs in which the carriers are classical particles except that Fermi-Dirac statistics is obeyed.[28] The result is that the current in a given lead m is, of course, linearly related to the voltage differences as in Eq. (1),

$$I_m = \sum_n c_{mn}(V_n - V_m) . \tag{A1}$$

After finding the c_{mn}, we shall see that the classical transmission coefficients defined by analogy with Eq. (1), $T_{mn} \equiv c_{mn} h/e^2$, correspond to one's intuitive notion of transmission probability. In obtaining these results, we closely follow methods used in the theory of point contact spectroscopy.[57]

The collisionless Boltzmann equation for the distribution function $f(\mathbf{r},\mathbf{k})$ is the natural starting point for a classical ballistic calculation

$$\frac{\mathbf{F}}{\hbar}\cdot\frac{\partial f}{\partial \mathbf{k}} + \frac{\hbar\mathbf{k}}{m}\cdot\frac{\partial f}{\partial \mathbf{r}} = 0 , \tag{A2}$$

where $\mathbf{F}$ is the force on the particle. The boundary conditions corresponding to injection from reservoirs can be written using the equilibrium Fermi distribution $f_0(\varepsilon) \equiv 1/(e^{\beta(\varepsilon-\mu_0)}+1)$. In terms of the chemical potential shift $\delta\mu_n$ of reservoir n with respect to the equilibrium μ_0.

$$f(\mathbf{r},\mathbf{k}) \rightarrow f_0(\varepsilon_k - \delta\mu_n) \tag{A3}$$

as $r \rightarrow \infty$ in lead n. In using this boundary condition we have assumed, as in the quantum Landauer approach,[21] that the leads of the ballistic region widen out into two-dimensional regions of definite chemical potential. This well-defined problem can be solved by the method of characteristics in which the left-hand side of Eq. (A2) is written as a total derivative along a classical trajectory $df/dt|_{\text{trajectory}} = 0$. Thus f is constant along each trajectory. For the linear response, the effect of the driving field on the trajectories is negligible and the particles follow essentially equilibrium trajectories. The solution for $f(\mathbf{r},\mathbf{k})$, then, is to follow each trajectory at $\mathbf{r}$, characterized by $\hat{\mathbf{k}}$, backwards in time until it is clear from which reservoir it came, say μ_n; this direction in k space at $\mathbf{r}$ is therefore filled to energy $\varepsilon_k = \mu_n$.

In making a connection between transport and transmission coefficients, one often assumes that the transition from the region of interest to the reservoirs is reflectionless.[21,33,58] Within this approximation, it is clear from the solution for the distribution function that the transmission probabilities through the junction region will determine the form of $f(\mathbf{r},\mathbf{k})$. Also, for the distribution function characterizing particles before entering the junction, any particle going towards the junction will have come from the reservoir attached to that lead (in the absence of a magnetic field); hence all forward-going trajectories are equally populated.[29]

The current is given by the integral of the current density over the cross section of the lead

$$I_m = e\int dy_m \int \frac{d^2k}{4\pi^2} v_{\parallel} f(y_m,\mathbf{k}) , \tag{A4}$$

where y_m is perpendicular to the lead direction. For simple junctions, this integral can be evaluated analytically, as in the case of a T or cross structure below, yielding expressions for the coefficients c_{mn} of Eq. (A1). For more complex situations, one can evaluate this integral in a

Monte Carlo fashion by simply tracing many particle trajectories.[28]

For the case of a cross structure (the $L=0$ limit of the structure in the inset to Fig. 9), it is straightforward to work out the transmission into lead 1 in terms of y_1 at the junction measured from lead 2 and the angular deviation from the direction of lead 1. The distribution function is

$$f(y_1,\mathbf{k})=\begin{cases} f_0(\varepsilon_k-\delta\mu_2), & \arctan(y_1/W)<\theta_k<\pi/2 \\ f_0(\varepsilon_k-\delta\mu_3), & \arctan(y_1/W-1)<\theta_k<\arctan(y_1/W) \\ f_0(\varepsilon_k-\delta\mu_4), & -\pi/2<\theta_k<\arctan(y_1/W-1)\ . \end{cases} \tag{A5}$$

Carrying out the integral for the current, one finds

$$I_1=\frac{e}{h}\frac{k_F W}{2\pi}[(2-\sqrt{2})(\mu_2-\mu_1)+(2-\sqrt{2})(\mu_4-\mu_1) +2(\sqrt{2}-1)(\mu_3-\mu_1)]\ . \tag{A6}$$

The transmission coefficients, therefore, are $T_{31}=(\sqrt{2}-1)k_F W/\pi$ and $T_{21}=(2-\sqrt{2})k_F W/2\pi$; of course, there is no reflection in the classical limit. A similar calculation for the T structure yields $T_{31}=(\sqrt{5}-1)k_F W/2\pi$, $T_{21}=(3-\sqrt{5})k_F W/2\pi$, and $T_{22}=(\sqrt{5}-2)k_F W/\pi$.

For the discrete-classical model, only discrete $\mathbf{k}$ are included in the integral for the current, Eq. (A4). Those included have $k_\perp=\pm i\pi/W$, where i is an integer up to the number of modes M, and one replaces $\int d^2k/4\pi^2$ by

$$\sum_{i=\pm1}^{\pm M}\int dk_{xi}/4\pi W\ .$$

This intuitively appealing way of partially taking into account the quantum mode structure can be justified from a WKB approximation for the Green function.[30]

APPENDIX B: THRESHOLD SINGULARITIES

In order to find the form of the threshold singularities in the transmission coefficients, we first write the scattering wave states in the asymptotic region which define these coefficients[23,24]

$$\psi^+_{n,\nu}(\mathbf{x})\rightarrow\begin{cases} e^{iq_\nu x}\chi_\nu(y)+\sum_\mu t_{nn}(\mu,\nu)(q_\nu/q_\mu)^{1/2}e^{-iq_\mu x}\chi_\mu(y), & \text{with } \mathbf{x} \text{ in lead } n \\ \sum_\mu t_{mn}(\mu,\nu)(q_\nu/q_\mu)^{1/2}e^{-iq_\mu x}\chi_\mu(y), & \text{with } \mathbf{x} \text{ in lead } m\ . \end{cases} \tag{B1}$$

Here the incoming mode is ν in lead n and the transverse wave functions χ are normalized to unity. The index m extends over all N_L leads; the sum over μ extends over the M open modes. The square-root factors ensure conservation of flux and hence a unitary S matrix in this multimode situation. The form of the threshold singularities follows from the regularity of ψ^+ as a function of the q_μ and, in particular, that it is analytic as a function of q_μ about $q_\mu=0$.[35,59]

We first consider the case of transmission from an open mode to a higher threshold mode, $\nu<\mu$ and $q_\mu\rightarrow0$. The wave function $\psi^+_{n,\nu}$ must not diverge in this limit from which one concludes

$$t_{mn}(\mu,\nu)\sim\sqrt{q_\mu}\ \text{ as } q_\mu\rightarrow0,\ \nu<\mu\ . \tag{B2}$$

The reciprocity relations for the transmission coefficients which come from time-reversal symmetry[19] immediately yield the relation for transmission from a threshold mode to a lower open mode (even in the presence of a magnetic field)

$$t_{mn}(\mu,\nu)\sim\sqrt{q_\nu}\ \text{ as } q_\nu\rightarrow0,\ \mu<\nu\ . \tag{B3}$$

Because of this square-root threshold behavior, $\psi^+_{n,\nu}$ is an analytic function near threshold in spite of the square-root factors in Eq. (B1).

When both the incoming and outgoing modes are at threshold, the square-root factors in Eq. (B1) are not present. The analyticity of ψ^+ implies that

$$t_{mn}(\nu,\nu)\sim c+q_\nu\ \text{ as } q_\nu\rightarrow0,\ \text{all leads } m\ . \tag{B4}$$

In fact, the constant term is present only for the reflection coefficient $m=n$ for which $c=-1$. The demonstration of this statement involves a rather complicated argument adapted from atomic scattering in which one matches an interior wave function onto the asymptotic behavior.[34,35]

Let the solution of Schrödinger's equation in the scattering region (which incorporates the junctions) be

$\psi(\mathbf{x})$ and consider its decomposition into modes at the boundary between the scattering region and the leads. We consider a scattering region large enough so that only the M propagating modes need to be considered, the evanescent modes having decayed near the junctions. Thus we introduce the functions

$$f_{n,\nu}(x_n) \equiv \int_{C_n} dy_n \, \psi(\mathbf{x}) \chi_\nu(y_n) \ , \tag{B5}$$

where C_n is the cross section in lead n at the boundary of the scattering region and y_n is the coordinate along this boundary. The asymptotic form of the wave function in Eq. (B1) implies that the logarithmic derivative of f is

$$\frac{f'_{m,\mu}}{f_{m,\mu}} = \frac{-iq_\mu (q_\nu/q_\mu)^{1/2} t_{mn}(\mu,\nu) e^{+iq_\mu L}}{(q_\nu/q_\mu)^{1/2} t_{mn}(\mu,\nu) e^{+iq_\mu L}} = -iq_\mu \ , \tag{B6}$$

except when $m=n$ and $\mu=\nu$ (i.e., reflection into the injected mode). The logarithmic derivatives in Eq. (B6) provides $N_L M - 1$ constraints on the interior wave function. However, the interior wave function is determined by $N_L M$ coefficients and one of these is the overall normalization which cannot be fixed by a logarithmic derivative. Thus the logarithmic derivative for $m=n$ and $\mu=\nu$, which is not included in Eq. (B6), is fixed to be equal to some complex constant C,

$$\frac{f'_{n,\nu}}{f_{n,\nu}} = \frac{iq_\nu [e^{-iq_\nu L} - t_{nn}(\nu,\nu) e^{-iq_\nu L}]}{e^{-iq_\nu L} + t_{nn}(\nu,\nu) e^{+iq_\nu L}} \equiv C \ . \tag{B7}$$

To find the behavior to lowest order as $q_\nu \to 0$, one evaluates C at threshold, $C_0 \equiv C(q_\nu = 0)$, and solves Eq. (B7) to lowest order in q_ν. The result for the intensity is

$$|t_{nn}(\nu,\nu)|^2 \approx 1 - 2iq_\nu \left[\frac{1}{C_0} - \frac{1}{C_0^*} \right] \ . \tag{B8}$$

Because the boundary conditions, Eq. (B6), on the interior problem are complex, C_0 is in general complex. We find, then, that the reflected intensity is 1 at threshold and that deviations from this above threshold are of order q_ν.

By unitarity, then, the transmission between different leads must be zero at threshold. Then from Eq. (B4) one has

$$t_{mn}(\nu,\nu) \sim q_\nu \ \text{ as } q_\nu \to 0, \ m \neq n \ . \tag{B9}$$

The deviation of the intensity is order of q_ν^2, a higher-order than that for the reflection coefficient. Unitarity near threshold is preserved since the transmission between different modes is of order q_ν, Eq. (B3).

An exception to the above argument occurs at the threshold for the first mode, $M=1$, when more than one lead has the same threshold (same width) and in the absence of a magnetic field. In this case, the right-hand side of Eq. (B6) is zero at threshold so that all the constraints on the interior wave function are real. A solution of Schrödinger's equation with real boundary conditions is real and hence C_0 is real. Thus the first-order deviations, Eq. (B8), vanish and one obtains

$$|t_{mn}(1,1)|^2 - \delta_{mn} \sim q_\nu^2 \ . \tag{B10}$$

The fact that the first-order term drops out of the reflected intensity is required by unitarity and the analyticity of the wave function.

The final case to consider is the singularity in $t_{mn}(\mu,\nu)$ at the threshold for mode $\eta > \mu,\nu$. Unitarity and the result for scattering into a threshold mode, Eq. (B2), yield

$$\sum_m \sum_{\mu=1}^{\eta-1} |t_{mn}(\mu,\nu)|^2 = 1 - \sum_m |t_{mn}(\eta,\nu)|^2 = 1 - \alpha q_\eta \ , \tag{B11}$$

where $\alpha > 0$ is a real constant. We assume that the deviation away from threshold is divided among all the different channels,

$$|t_{mn}(\mu,\nu)|^2 = |t^0_{mn}(\mu,\nu)|^2 + \beta q_\eta, \quad E > E_\nu \ , \tag{B12}$$

where the superscript 0 denotes the value at threshold and the sign of β is not fixed. In terms of an unknown phase δ and a real parameter γ, the transmission coefficient is

$$t_{mn}(\mu,\nu) = t^0_{mn}(\mu,\nu)(1+\gamma q_\eta) e^{i\delta} \ . \tag{B13}$$

The phase δ must be real for $E > E_\eta$ and linear in q_η, $\delta \approx b q_\eta / 2$. The analytic continuation of Eq. (B13) to energies below threshold $E < E_\eta$ is

$$|t_{mn}(\mu,\nu)|^2 = |t^0_{mn}(\mu,\nu)|^2 (1 + \gamma^2 |q_\eta|^2) e^{-b|q_\eta|} \ , \tag{B14}$$

which to first order in q_η yields

$$|t_{mn}(\mu,\nu)|^2 = |t^0_{mn}(\mu,\nu)|^2 (1 - b|q_\eta|), \quad E < E_\nu \ . \tag{B15}$$

Four possible forms for the threshold singularity are possible (Fig. 4) and are determined by the signs of γ and b in Eqs. (B13) and (B15).[34,35]

This completes the deviation of the threshold singularities. The main results, Eqs. (B2), (B3), (B8), (B9), (B12), and (B15), are summarized in the main text as Eqs. (3) and (4).

APPENDIX C: MEAN FREE PATHS IN A WAVEGUIDE

When one introduces elastic scattering through a disordered potential, it is useful to characterize the strength of the scattering through a mean free path for the particles. In working out this quantity, we assume that the density of impurities n is low so that the mean free path l is related to the cross section of a single scatterer σ by $l = 1/n\sigma$. The situation that we consider is a single waveguide of width W containing a small scattering region of length L. We will express the cross section in terms of transmission coefficients and thus obtain expressions for l.

The cross section of a single scatterer is the ratio of the total rate of scattered intensity to the input flux given equal input flux in all modes. By definition of the transmission coefficients, the intensity scattered into mode μ from mode ν is proportional to $R(\mu,\nu)$ for reflection and $T(\mu,\nu)$ for $\mu \neq \nu$ in the case of forward

scattering. For forward scattering from mode ν to itself, one must separate out the scattered part from the part unaffected by the potential. The scattered amplitude is $t(\nu,\nu)-1$ so that the scattered intensity is $T(\nu,\nu)+1-2\,\mathrm{Re}[t(\nu,\nu)]$. Summing over the contributions of all the modes, one finds that the cross section is given by

$$\sigma=\frac{W}{M}\sum_{\nu}\left[\sum_{\mu}R(\mu,\nu)+\sum_{\mu\neq\nu}T(\mu,\nu)+T(\nu,\nu)+1-2\,\mathrm{Re}[t(\nu,\nu)]\right]. \quad \text{(C1)}$$

The sums can be performed using the unitarity conditions to yield[60]

$$\sigma=\frac{2W}{M}\left[M-\sum_{\nu}\mathrm{Re}[t(\nu,\nu)]\right]. \quad \text{(C2)}$$

The density of this scattering site is $1/LW$ so the mean free path is

$$l_{\mathrm{tot}}=\frac{1}{n\sigma}=\frac{ML}{2\left[M-\sum_{\nu}\mathrm{Re}[t(\nu,\nu)]\right]}. \quad \text{(C3)}$$

Because backscattering degrades the current more effectively than forward scattering, the mean free path relevant to transport is not the total mean free path found above, but one in which the different scattering processes are weighted according to their effectiveness. In the bulk semiclassical limit this corresponds to the well-known $1-\cos\theta$ term in the transport mean free path. In the case of waveguides, the scattering between forward-going modes does not degrade the current at all, while the effectiveness of scattering into backward-going modes does not depend on the mode number. Thus we are led to weight the reflection coefficients by a factor of 2 in carrying out the sum in Eq. (C1) while weighting the transmission coefficients by zero. This yields the result for the backscattering mean free path

$$l_{\mathrm{bs}}=\frac{ML}{2\sum_{\nu}\sum_{\mu}R_{\mu,\nu}}. \quad \text{(C4)}$$

This result corresponds to the semiclassical mean free path used recently by Glazman and Jonson,[5] where all scattering from forward-going states into backward-going states is weighted equally. Equations (C3) and (C4) were used in evaluating the mean free paths in connection with Fig. 14.[50]

*Present address: AT&T Bell Laboratoires, 600 Mountain Ave., Murray Hill, New Jersey 07974.

[1]For reviews, see *Physics and Technology of Submicron Structures,* edited by H. Heinrich, G. Bauer, and F. Kuchar (Springer-Verlag, Berlin, 1988); *Nanostructure Physics and Fabrication,* edited by M. A. Reed and W. P. Kirk (Academic, New York, 1989).

[2]G. Timp, A. M. Chang, P. Mankiewich, R. Behringer, J. E. Cunningham, T. Y. Chang, and R. E. Howard, Phys. Rev. Lett. **59**, 732 (1987).

[3]M. Shayegan, V. J. Goldman, M. Santos, T. Sajoto, L. Engle, and D. C. Tsue, Appl. Phys. Lett. **53**, 2080 (1988); L. N. Pfeifer, K. W. West, H. L. Stormer, and K. W. Baldwin, *ibid.* **55**, 1880 (1989); C. T. Foxon, J. J. Harris, D. Hilton, J. Hewitt, and C. Roberts, Semicond. Sci. Technol. **4**, 582 (1989).

[4]J. A. Nixon and J. H. Davies, Phys. Rev. B **41**, 7929 (1990); J. H. Davies, J. A. Nixon, and H. U. Baranger, in *Condensed Systems of Low Dimensionality,* edited by J. L. Beeby (Plenum, New York, in press).

[5]L. I. Glazman and M. Jonson (private communication).

[6]F. Lenz, J. T. Londergan, E. J. Moniz, R. Rosenfelder, M. Stingl, and K. Yazaki, Ann. Phys. (N.Y.) **170**, 65 (1986).

[7]G. Timp, H. U. Baranger, P. deVegvar, J. E. Cunningham, R. E. Howard, R. Behringer, and P. M. Mankiewich, Phys. Rev. Lett. **60**, 2081 (1988).

[8]R. L. Schult, D. G. Ravenhall, and H. W. Wyld, Phys. Rev. B **39**, 5476 (1989); D. G. Ravenhall, H. W. Wyld, and R. L. Schult, Phys. Rev. Lett. **62**, 1780 (1989).

[9]Y. Avishai and Y. B. Band, Phys. Rev. Lett. **62**, 2527 (1989).

[10]G. Kirczenow, Solid State Commun. **71**, 469 (1989); Phys. Rev. Lett. **62**, 2993 (1989); Solid State Commun. **74**, 1051 (1990).

[11]F. M. Peeters, Superlattices Microstructures **6**, 217 (1989); in *Science and Engineering of 1- and 0-Dimensional Semiconductors,* edited by S. P. Beaumont and C. M. Sotomayor-Torres (Plenum, New York, 1990).

[12]F. Sols, M. Macucci, U. Ravaioli, and K. Hess, Appl. Phys. Lett. **54**, 350 (1989); F. Sols, K. Hess, U. Ravaioli, and M. Macucci, J. Appl. Phys. **66**, 3892 (1989).

[13]S. Datta, Superlattices Microstructures **6**, 83 (1989).

[14]P. Exner, Phys. Lett. A **141**, 213 (1989); P. Exner and P. Seba, J. Math. Phys. **30**, 2574 (1989).

[15]P. F. Bagwell, Phys. Rev. B **41**, 10 354 (1990); (unpublished).

[16]C. S. Lent, Appl. Phys. Lett. **56**, 2554 (1990); (unpublished).

[17]A. Weisshaar, J. Lary, S. M. Goodnick, and V. K. Tripathi, SPIE Proc. (to be published).

[18]R. L. Schult, H. W. Wyld, and D. G. Ravenhall, Phys. Rev. B **41**, 12 760 (1990).

[19]M. Büttiker, Phys. Rev. Lett. **57**, 1761 (1986).

[20]H. U. Baranger and A. D. Stone, in *Science and Engineering of 1- and 0-Dimensional Semiconductors* (Ref. 11), p. 121.

[21]R. Landauer, IBM J. Res. Dev. **1**, 233 (1957); Z. Phys. B **68**, 217 (1987).

[22]D. S. Fisher and P. A. Lee, Phys. Rev. B **23**, 6851 (1981).

[23]A. D. Stone and A. Szafer, IBM J. Res. Dev. **32**, 384 (1988).

[24]H. U. Baranger and A. D. Stone, Phys. Rev. B **40**, 8169 (1989).

[25]P. A. Lee and D. S. Fisher, Phys. Rev. Lett. **47**, 882 (1981); D. J. Thouless and S. Kirkpatrick, J. Phys. C **14**, 235 (1981); A. MacKinnon, Z. Phys. B **59**, 385 (1985).

[26]H. U. Baranger, A. D. Stone, and D. P. DiVincenzo, Phys. Rev. B **37**, 6521 (1988).

[27]H. U. Baranger and A. D. Stone, Phys. Rev. Lett. **63**, 414 (1989).

[28]C. W. J. Beenakker and H. van Houten, Phys. Rev. Lett. **63**, 1857 (1989); in *Electronic Properties of Multilayers and Low-Dimensional Semiconductor Structures,* edited by J. M. Chamberlain, L. Eaves, and J. C. Portal (Plenum, New York, 1990).

[29]This corresponds to an "injection distribution" of $\cos\theta$ for a

time-dependent problem as in Beenakker and van Houten, Ref. 28.

[30]R. A. Jalabert, H. U. Baranger, and A. D. Stone, Phys. Rev. Lett. (to be published).

[31]B. J. van Wees, H. van Houten, C. W. J. Beenakker, J. G. Williamson, L. P. Kouwenhoven, D. van der Marel, and C. T. Foxon, Phys. Rev. Lett. **60**, 848 (1988).

[32]D. A. Wharam, T. J. Thornton, R. Newbury, M. Pepper, H. Ajmed, J. E. F. Frost, D. G. Hasko, D. C. Peacock, D. A. Ritchie, and G. A. C. Jones, J. Phys. C **21**, L209 (1988).

[33]L. I. Glazman, G. B. Lesovick, D. E. Kmelnitskii, and R. I. Shekhter, Pis'ma Zh. Eksp. Teor. Fiz. **48**, 218 (1988) [JETP Lett. **48**, 238 (1988)].

[34]L. D. Landau and E. M. Lifshitz, *Quantum Mechanics* (Pergamon, New York, 1977), pp. 523–529, 542–546, 591–620.

[35]A. I. Baz, Y. B. Zel'dovich, and A. M. Perelomov, *Scattering, Reactions, and Decay in Nonrelativistic Quantum Mechanics* (Israel Program for Scientific Translations, Jerusalem, 1969), pp. 147–192.

[36]Y. Takagaki, K. Gamo, S. Namba, S. Ishida, S. Takaoka, M. Murase, K. Ishibashi, and Y. Aoyagi, Solid State Commun. **68**, 1051 (1988).

[37]Y. Takagaki, K. Gamo, S. Namba, S. Takaoka, M. Murase, and S. Ishida, Solid State Commun. **71**, 809 (1989).

[38]R. E. Behringer, G. Timp, H. U. Baranger, and J. E. Cunningham, Solid State Commun. **75**, 873 (1990).

[39]Y. Takagaki, K. Gamo, S. Namba, S. Takaoka, and K. Murase, Solid State Commun. **75**, 873 (1990).

[40]L. I. Glazman and I. A. Larkin (unpublished).

[41]P. L. McEuen, T. E. Kopley, and R. G. Wheeler, Bull. Am. Phys. Soc. **34**, 778 (1989).

[42]The power spectra here are calculated using an all-poles method of order 60. See W. H. Press, B. P. Flannery, S. A. Teukolsky, and W. T. Vetterling, *Numerical Recipes* (Cambridge University Press, Cambridge, England, 1986), pp. 430–435.

[43]M. L. Roukes, A. Scherer, and B. P. Van der Gaag, Phys. Rev. Lett. **64**, 1154 (1990).

[44]The classical values for the resistances and transmission coefficients in the double-junction case are $T_{31}=0.480$, $T_{21}=0.137$, $T_{41}=0.383$, $T_{22}=0.236$, $T_{24}=0.245$, $R_{\rm LONG}=0.339$, and $R_{\rm NL}=0.265$, where the unit of transmission is $k_F W/\pi$ and the unit of resistance is $h\pi/e^2 k_F W$. These values are calculated by tracing many particles through the junctions as in Ref. 28; the statistical error is ± 1 in the last digit for the transmission coefficients and ± 3 for the resistances.

[45]J. Leo and A. H. MacDonald, Phys. Rev. Lett. **64**, 817 (1990), and references therein.

[46]G. Timp and A. M. Chang (private communications), and Ref. 2. Note also Takagaki *et al.*, Ref. 39.

[47]Recent experiments have shown that the resistance fluctuations caused by impurity scattering are nonlocal over a phase-breaking length. Here, however, we are dealing with an average resistance effect, not a fluctuation, which therefore decays over a mean free path.

[48]L. W. Molenkamp, A. A. M. Staring, C. W. J. Beenakker, R. Eppenga, C. E. Timmering, J. G. Williamson, C. J. P. M. Harmans, and C. T. Foxon, Phys. Rev. B **41**, 1274 (1990).

[49]S. Das Sarma and F. Stern, Phys. Rev. B **32**, 8442 (1985); F. F. Fang, T. P. Smith, and S. L. Wright, Surf. Sci. **196**, 1988 (1988).

[50]Evaluation of these mean free paths was carried out in waveguides described by tight-binding Hamiltonians where the disorder was introduced as a random on-site term. In the case of the standard Anderson model where each site energy is random, the two mean free paths agreed to within the statistical error ($\approx 10\%$), showing that the scattering is largely isotropic in this case. For the smoother potential used here, every fifth lattice energy is chosen at random from a uniform distribution between $-\alpha/2$ and $\alpha/2$. Intermediate energies were obtained by interpolation and 5 five-site units were used as the single scatterer for the mean-free-path calculations. The waveguide was 21 sites wide with $\alpha=0.18$, $l_{\rm tot}=140\pm 3$ sites, and $l_{\rm bs}=1230\pm 42$ for $k_F W/\pi=4.5$.

[51]The decay of $R_{\rm NL}$ due to the relaxation of the transverse momenta is similar to the asymmetry and broadening of the transmission in the resonant tunneling case when transverse scattering is included. See Ref. 45.

[52]A. Kumar, S. E. Laux, and F. Stern, Appl. Phys. Lett. **54**, 1270 (1989).

[53]For a review of quantum point contacts, see H. van Houten, C. W. J. Beenakker, and B. J. van Wees, in *Semiconductors and Semimetals,* edited by M. A. Reed (Academic, New York, in press).

[54]T. J. Thornton, M. L. Roukes, A. Scherer, and B. P. Van der Gaag, Phys. Rev. Lett. **63**, 2128 (1989).

[55]H. U. Baranger and A. D. Stone, Surf. Sci. **229**, 212 (1990).

[56]M. L. Roukes and O. L. Alerhand, Phys. Rev. Lett. **65**, 1651 (1990).

[57]I. O. Kulik, A. N. Omel'yanchuk, and R. I. Shekter, Fiz. Nizk. Temp. **3**, 1543 (1977) [Sov. J. Low Temp. Phys. **3**, 740 (1977)]; A. G. M. Jansen, A. P. van Gelder, and P. Wyder, J. Phys. C **13**, 6073 (1980).

[58]Y. Imry, in *Perspectives on Condensed Matter Physics,* edited by G. Grinstein and E. Mazenko (World Scientific, Singapore, 1986).

[59]The scattering wave function ψ^+ cannot, of course, be analytic everywhere as a function of q_η. It depends on all the q_μ and therefore must have branch cuts at the thresholds for the μ modes.

[60]This equation is the optical theorem in the waveguide context. Note that the real part of the forward-scattering amplitude occurs rather than the usual imaginary part. This is caused by a different choice of the relative phase of the incoming wave and the scattered wave in the same direction. In the waveguide context this phase is zero since both the incoming and the scattered wave are $\exp(ikx)$. In the usual three-dimensional case the scattered wave is $\exp(i|k|\,|r|)/|r|$; the part of this wave in the forward direction is out of phase with the incoming $\exp(i\mathbf{k}\cdot\mathbf{r})$. The extra factor of i accounts for the change from the imaginary part in the usual context to the real part here.